A model of early evolution of karst conduits affected by subterranean CO_2 sources

F. Gabrovšek · B. Menne · W. Dreybrodt

Abstract In investigating early karstification of one-dimensional conduits by computer models, so far one has assumed that the CO_2 content of the calcite aggressive water stems entirely from the surface. Subterranean sources of CO_2, however, can rejuvenate the solutional power of water already close to equilibrium with respect to calcite, and boost dissolution rates. In a first scenario we have investigated the influence of a punctual source of CO_2 as the most simple case of release of CO_2 into a karstifiable fracture at some position KL from its entrance of the widening joint with length L, ($K < 1$). The results show that only a small increase of the p_{CO_2} in the solution to about 0.01 atm is sufficient to reduce the breakthrough times to about 0.3 with respect to the case, where no CO_2 is delivered. Other sources of CO_2 are due to the metabolic activity of microorganisms. The existence of such diverse subterraneous microbial life in karst systems is demonstrated. Whether situated on the fissure surfaces or free floating in the karst water, one basic product of their metabolism is CO_2. This contributes over the whole flow path to the p_{CO_2} of the karst water. Therefore in a second scenario we assumed a constant rate of CO_2-input along parts of the fracture, as could be delivered by the activity of aerobic bacteria dwelling at its walls. Such a scenario also applies to an extended diffuse CO_2 migration from volcanic activity deep underground. In this case drastic reductions of the breakthrough time by about one order of magnitude are observed. These reductions are enhanced when the fracture aperture width of the initial fracture decreases. The physicochemical mechanisms of enhancement of karstification are discussed in detail by considering the evolution of the fracture aperture width and of the dissolution rates in space and time.

Key words Karst · Speleogenesis · Subterranean · CO_2 · Limestone dissolution

Received: 17 December 1998 · Accepted 23 April 1999

F. Gabrovšek · W. Dreybrodt (✉)
Institute of Experimental Physics, University of Bremen,
D-28334 Bremen, Germany,
e-mail: dreybrod@physik.uni-bremen.de

F. Gabrovšek
Karst Research Institute, ZRC-SAZU, Postojna, Slovenia

B. Menne
BIUS, Hartfeldstr. 32, D-75417 Mühlacker, Germany

Introduction

Karst processes are driven by chemical, physical, and hydrogeological forces. Figure 1 schematically illustrates an uplifted limestone block, which is dissected by various primary fractures such as joints and bedding planes at the onset of karstification. Some of these comprise percolating pathways from the upper surface to a valley. Through these, the surface water present at some input points at the top is driven down to the valley. The solutional attack of this CO_2-containing water widens these

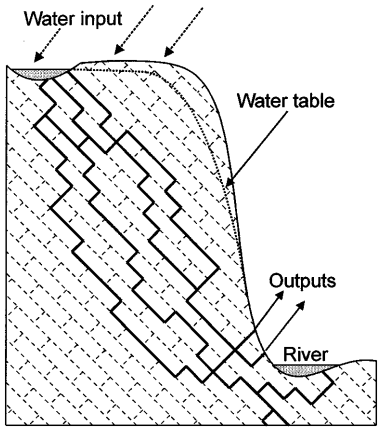

Fig. 1
Schematic drawing of a karst aquifer in its initial state. The *full lines* represent a net of percolating pathways consisting of narrow initial fractures which transmit water from the input to the outputs

fractures by chemical dissolution of the bedrock and underground drainage networks may result (Dreybrodt 1988; Ford and Williams 1989; White 1988).

To understand the evolution of karstification on its scales in space and time one has to specify by which parameters these processes are determined. To this end, first models have been put forward (Dreybrodt 1988, 1990, 1996; Dreybrodt and Gabrovsek 1999a; Groves and Howard 1994a,b; Howard and Groves 1995; Palmer 1984, 1991, 1999; Siemers and Dreybrodt 1998; Dreybrodt and Siemers 1999) which investigate the evolution of the aperture widths of one-dimensional fractures with initial even spacing. They all replace the complicated natural fractures by a plane parallel fracture of length L, initial aperture width a_0 of a few tenths of a millimeter, and width b_0 in the order of meters. The hydraulic head h acting at the entrance drives CO_2-containing, calcite aggressive water through this fracture, thus widening its aperture by dissolution. The rates at which this happens are governed by the dissolution kinetics of limestone, which are given by

$$F(c) = k_1(1 - c/c_{eq}) \text{ for } c < c_s \quad (1a)$$

and

$$F(c) = k_n(1 - c/c_{eq})^n \text{ for } c \geq c_s \quad (1b)$$

k_1 and k_n are rate constants in $\text{mol}\cdot\text{cm}^{-2}\cdot\text{s}^{-1}$ c is the concentration of Ca^{2+} ions and c_{eq} their equilibrium concentration with respect to calcite in mole/cm^3. At the concentration c_s, the rates switch from a linear rate law to higher order kinetics with exponent n. Depending on the lithology of the specific limestone n varies between 3 and 11 (Eisenlohr and others 1997, 1999). The switch concentration c_s is about 0.7 c_{eq} to 0.9 c_{eq}. This rate law has first been suggested by Palmer (1984), and later experimentally proven to be valid for dissolution of limestone under the conditions of a closed system with respect to CO_2, as it occurs in a completely water filled fracture (Eisenlohr and others 1997, 1999). It must be stressed at this point that this non-linear rate law is essential to the evolution of karst. Under the action of solely a linear rate law, karstification cannot proceed in geological time scales (Dreybrodt and Gabrovsek 1999a).

Figure 2 shows the evolution of a one-dimensional karst conduit with an initial aperture width of $a_0 = 0.02$ cm, $b_0 = 100$ cm, $L = 10^5$ cm, and a hydraulic gradient $i = h/L = 0.05$. The equilibrium concentration is $c_{eq} = 2\cdot10^{-6}$ mole/cm^3 as it commonly occurs in karst waters. The inflowing solution has a concentration $c = 0$. The rate constants $k_1 = 4\cdot10^{-11}$ $\text{mol}\cdot\text{cm}^{-2}\cdot\text{s}^{-1}$, and $k_n = 4\cdot10^{-8}$ $\text{mol}\cdot\text{cm}^{-2}\cdot\text{s}^{-1}$ are typical values obtained from laboratory experiments under the conditions of a closed system at 10 °C (Dreybrodt and Eisenlohr 1999, Eisenlohr and others 1997, 1999). We refer to this as the standard later on.

Figure 2a in a logarithmic plot depicts the flow rate through the fracture as a function of time. Initially there is a slow increase which is enhanced in time until the flow rates are drastically accelerated to such an amount that they exceed the water available at the surface (cf. Fig. 1). At this breakthrough time T_B^0 the hydraulic head breaks down and the initial phase of laminar flow through the fracture is terminated.

Figure 2b represents the evolution of the aperture widths along the fracture for various times. During the first 90% of T_b^0 widening of the fracture is restricted to its entrance, and only a slow increase of its aperture width is observed at the exit, until close to breakthrough a dramatic widening occurs. This behavior is mirrored by Fig. 2c, which shows the concentration of Ca^{2+} along the fracture (note the logarithmic scale). During most of the time it rises quickly at the entrance until c_s is achieved after a short distance compared to the length. From thereon higher order dissolution kinetics, active along almost the entire length of the fracture, determines the evolution of its aperture width. Then, at breakthrough, the concentration drops to a value close to zero. Further dissolution is then governed by the first order kinetics and widening is uniform along the entire fracture. Fig. 2d depicts the dissolution rates along the fracture. In the region of linear kinetics (cf. Eq. 1a) close to the entrance the rates drop exponentially, as long as first order kinetics is active. Beyond the point c_s where the rates are nonlinear (cf. Eq. 1b), they drop much slower with a hyperbolic law, such that a small but still significant dissolutional widening exists at the exit. The rates at the exit increase with time due to increasing flow, and the region of first order dissolution slowly penetrates into the fracture with accelerated speed, until breakthrough occurs. Details of this dynamic behavior are given in the literature (Dreybrodt 1996, 1998; Dreybrodt and Gabrovsek 1999a).

It should be noted at this point that this behavior is not affected as long as the inflowing solution has a finite concentration $c_0 \leq c_s$, since during 90% of the time needed for breakthrough the higher order kinetics is active along almost the entire length of the fracture (Dreybrodt 1996; Dreybrodt and Gabrovsek 1999a). The time to achieve breakthrough is governed by a positive feedback mechanism. Widening at the exit increases flow rates due to the Hagen-Poisseuille law of laminar flow with approximately $a^3(L,t)$, where $a(L,t)$ is the aperture width at the exit. This increased rate enhances the dissolution rate at the exit thus causing further acceleration of flow rates until breakthrough occurs. A thorough mathematical analysis gives an upper limit approximation for the breakthrough time as

$$T_B^0 = \frac{(n-1)\cdot a_0}{(2n+1)\cdot 2\gamma\cdot F(L,0)} \quad (2)$$

$\gamma = 1.17\cdot10^9$ $\text{cm}^3\ \text{s}^{-1}$ year mol^{-1} converts the dissolution rate $F(L,0)$ at the exit of the fracture at $t = 0$ from $\text{mol}\cdot\text{cm}^{-2}\cdot\text{s}^{-1}$ to removal of bedrock in cm/year. T_B is given in years. Thus breakthrough occurs, when the aperture width at the exit has increased to several times of its initial value (Dreybrodt 1996; Dreybrodt and Gabrovsek 1999a, b). By calculating $F(L,0)$ for the initial fracture with even spacing a_0 and length L, one obtains

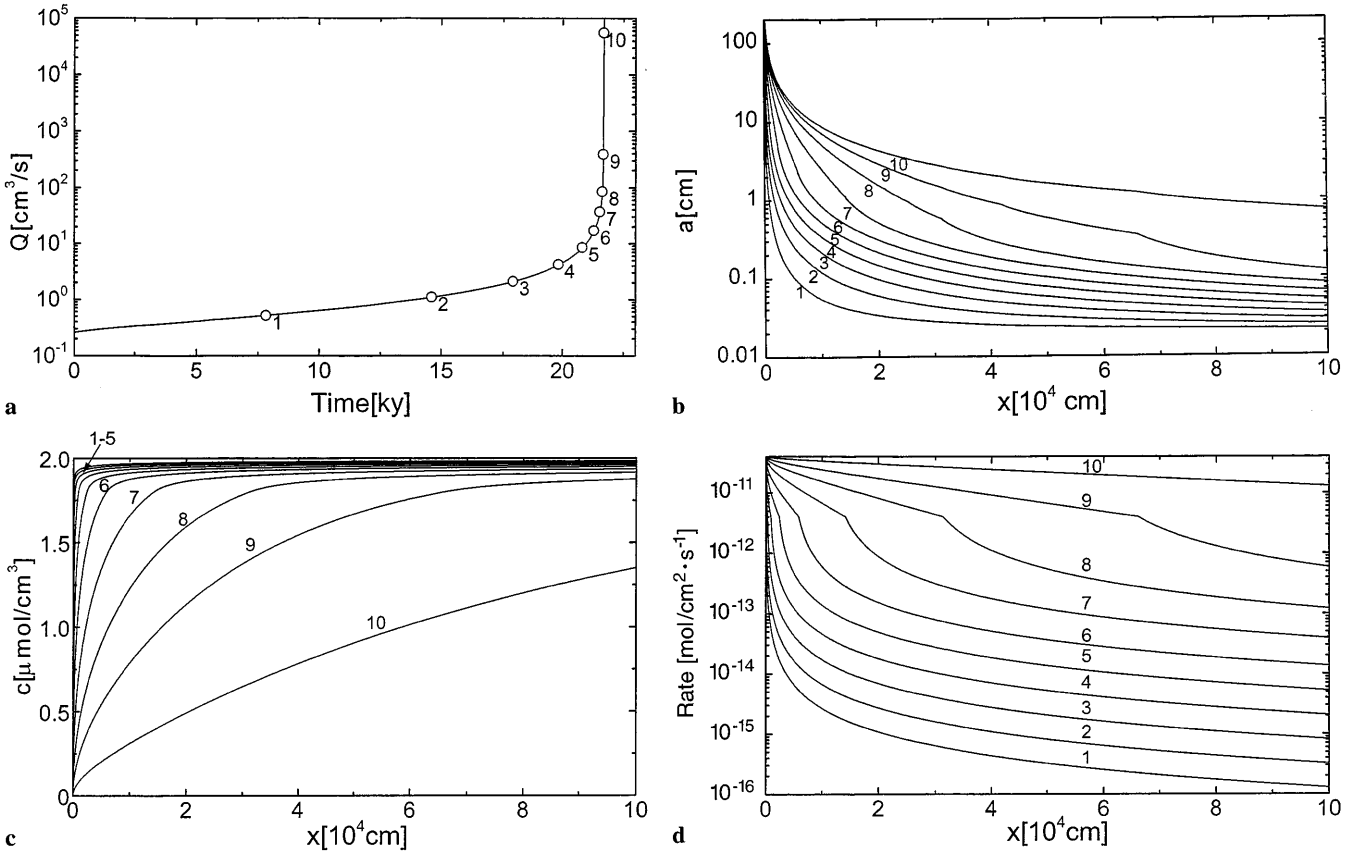

Fig. 2
Evolution of the standard fracture: $a_0 = 0.02$ cm, $b_0 = 100$ cm, $L = 10^5$ cm, $i = 0.05$, $k_1 = 4 \cdot 10^{-11}$ mol·cm^{-2}·s, $k_4 = 4 \cdot 10^{-8}$ mol·cm^{-2}·s, $n = 4$, $c_s = 0.9 c_{eq}$, $c_{eq} = 2 \cdot 10^{-6}$ mol/cm^3. **a** Evolution of the flow rate as a function of time. *Open circles* mark the points where the profiles in Figs. 2b–d are shown. The steep increase of the flow rate marks breakthrough time. Note logarithmic scale on Q(t). **b** Profiles of the aperture widths $a(x)$ recorded at various times: 7840, 14620, 17920, 19840, 20820, 21300, 21540, 21640, 21680 and 21700 years, labeled from 1–10 respectively. Times are chosen so, that the flow rate Q between two successive times doubles. Note logarithmic scale in aperture widths. Note the dramatic increase in aperture widths at breakthrough. **c** Concentration profiles along the fracture at times given above. The concentration front, i.e. the steep increase in concentration moves slowly towards the exit, such that during almost the entire time of evolution the concentration is $c > c_s$, and fourth order kinetics is active along almost the entire length of the conduit. Only close to the entrance first order kinetics ($c < c_s$) is operative. **d** Dissolution rates along the fracture at times given above

$$T_B^0 \approx \frac{1}{2\gamma} \cdot \frac{n-1}{2n+1} \cdot \left(\frac{1}{a_0}\right)^{\frac{2n+1}{n-1}} \left(\frac{24\eta L(n-1)}{\rho g i c_{eq}}\right)^{\frac{n}{n-1}} (k_n)^{\frac{1}{n-1}} \quad (3)$$

η is the viscosity of the water, ρ its density, and g earth's gravitational acceleration. Using units in g, cm, s, mole/cm^3 one obtains T_B^0 in years (cf. Table 1).
This equation specifies breakthrough time as a function of the parameters determining the evolution of karst.

Breakthrough time can be regarded as a measure of the degree of karstification in the sense that more highly karstified regions are expected, if breakthrough occurs in shorter times. The consequences of Eq. 3 to the understanding of karstification have been discussed in detail elsewhere (Dreybrodt 1996; Dreybrodt and Gabrovsek 1999a; Dreybrodt and Siemers 1999; Siemers and Dreybrodt 1998). It should be noted here that completely smooth even-spaced fractures are an idealization and do not occur in nature. It has been shown, however, that even considerable natural roughness of the fractures has no influence to the general pattern of early karst evolution, and only little influence to the value of the breakthrough time (Dreybrodt and Gabrovsek 1999b).
Up to now, in all the computer models of early karstification one has assumed that the CO_2-content of the calcite aggressive solution originates entirely from the surface water and that no additional sources of carbon dioxide exist underground, delivering CO_2 to the solution, when it flows within the fracture.
Extra sources of CO_2, however, can be supplied by: (a) volcanic release of CO_2 into a karstifiable region; (b) heterotrophic microorganisms dwelling at the walls of the fracture oxidize organic carbon constituents of karst water by aerobic metabolism to produce CO_2 along the flow path of the water.
Biogenic sources of carbon dioxide are due to the metabolic activity of microorganisms. Recent studies on subsurface sediments have suggested that bacterial popula-

Table 1
Parameters used in the model

Basic parameters		
Description	Name	Unit
Aperture width	a_0	cm
Width	b_0	cm
Fracture length	L	cm
Hydraulic gradient	i	
Linear kinetic constant	k_1	$mol \cdot cm^{-2} \cdot s^{-1}$
Nonlinear kinetic order	n	
Nonlinear kinetic constant	k_n	$mol \cdot cm^{-2} \cdot s^{-1}$
Switch concentration	c_s	mol/cm^3
Equilibrium concentration	c_{eq}	mol/cm^3
Viscosity of the solution	η	g/cms
Density of the solution	ρ	g/cm^3
Additional parameters for the point CO_2 sources		
Description	Name	Definition
Position of the CO_2 source	K	$x_{in} = K \cdot L,\ K \leq 1$
Ratio between c_{eq} before and after CO_2 input	α	c_{eq1}/c_{eq2}
Additional parameters for the extended CO_2 sources		
Description	Name	Definition
Region of the additional CO_2 input	K	$0 < x_{in} < K \cdot L$
	K_1, K_2	$K_1 \cdot L < x_{in} \leq K_2 \cdot L$
Total change of c_{eq} due to the CO_2 input	Δc_{eq}	$c_{eq2} - c_{eq1}$

tions which grow and survive in nutrient poor conditions, can respond to a wide range of nutrient concentrations, and are able to use a variety of organic substrates (Kazumi and Capone 1994).
Studies of organic matter in bed sediments reveal that biofilms together with the accompanying micro-fauna are quantitatively and most probably also qualitatively, the most important organic matter manifestation in this habitat. The spatial distribution of organic carbon (TOC) and organic nitrogen (TON) indicate the importance of water currents. In all the examined locations with lower water currents or throughflows in bed sediments, TOC contents are much higher. Biofilms are also important retention mechanisms buffering the pulsed organic matter imports (Leichtfried 1995). Bacteria and biofilms are ubiquitous in the subsurface of karstic landscapes. The mobile part of the subsurface biocenosis is represented mainly by the karst water biocenosis, the sessile part by the biofilms at the fissure surfaces and sediments. Fissure systems with diffuse flow reveal very good conditions for microbial life. Deceased microorganisms constitute accumulation of readily biodegradable material and will give rise to succession and microbial metabolism. A study performed in the Northern Limestone Alps reveals, that the subsurface microorganisms may be foremost associated with biofilms around sediment particles and bedrock surfaces (Menne and Rückert 1988; Menne 1997a,b, 1998). The basic biogeochemical mechanisms in karst systems with respect to rock dissolution – carbonatolyse and bioconservation – are described in Menne (1998). Patterns of microbial activity may be related to hydraulic gradients and flows of organic matter. Dissolved levels of O_2 and TOC influence the amount of organic matter transformed.
Concerning the nutritional situation, it is interesting that microorganisms are also known as inhabitants of ultrapure water. Due to the fact that karst water often reveals DOC-contents of 2 or more mg/l, microbial life is easily possible. There are pioneer bacteria, which can grow with DOC-values of less than 10 µg/l (Morita 1985). It is proposed, that temperature has little effect on growth in resource rich environments but a strong effect in resource poor environments (Felip and others 1996).
One limiting resource is phosphate. Shang and others (1996) demonstrated that especially *Pseudomonas spec.* are able to use phosphates adsorbed to surfaces.
As known from surface environments, generally all kinds of microorganisms are able to attack materials by the exudation and exhalation of metabolic products. Processes leading to material deterioration are quite complex, including physical, chemical and biological factors. In karst systems bacteria influence the equilibrium status of the CO_2–HCO_3^-–$CaCO_3$ system. In this paper we concentrate only on one possible metabolic result of microbial life, the carbon dioxide. Parameters of metabolism, which are correlated with growth or respiration of bacterial cells (oxygen uptake, production of carbon dioxide or acids) might be an adequate measurement for bacterial biomass. These testing methods are indicated in case other tests fail, e.g. at very low cell densities. Therefore the model calculations relate directly to microbial activity. Considering the dimension of the standard fissure in comparison with the dimension of bacterial cells, the cells are about two orders of magnitude smaller than the standard fissure aperture widths.
In this paper we will discuss the influence of the above mentioned CO_2-sources on the breakthrough times and thus to the intensity of karstification.

Punctual sources of CO_2

In a first scenario we assume an idealized punctual source of CO_2 at some distance $x_{in} = K \cdot L$ ($K \leq 1$), from the entrance of the fracture. This could apply to the most simple case of volcanic release of CO_2, which supplied to the calcite aggressive solution at that point increases its equilibrium value with respect to calcite by Δc_{eq}. The dissolution rates for $x < x_{in} = K \cdot L$ are determined by c_{eq1}, the equilibrium concentration related to the CO_2-concentration of the inflowing water. For $x > x_{in}$, one has to replace c_{eq1} by $c_{eq2} = c_{eq1} + \Delta c_{eq}$, since the equilibrium concentration increases due to the sudden increase of CO_2-concen-

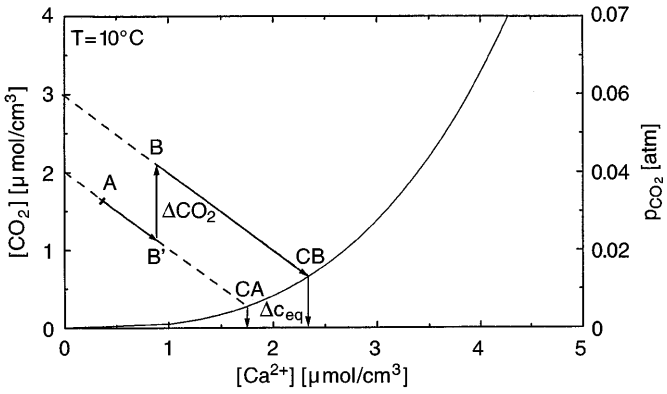

Fig. 3
Chemical evolution of a $H_2O-CaCO_3-CO_2$ solution flowing in a fracture under closed system conditions with respect to CO_2. The limiting curve represents equilibrium with respect to calcite. See text

tration supplied from the punctual CO_2-input at x_{in}. This idealized scenario gives first insight into the processes underlying the model.

Figure 3 shows a plot of the equilibrium curve of c_{eq} with respect to the actual concentration of CO_2 in an H_2O-$CaCO_3$ solution (Dreybrodt 1988). All points above this curve are related to an undersaturated solution. Point A designates water entering the fracture at $x=0$ with initial concentation $[Ca^{2+}]_{in}$ and $[CO_2]_{in}$. When this water flows down the fracture, CO_2 is consumed by dissolution of calcite under closed system conditions with respect to CO_2. By stoichiometry one molecule of CO_2 is converted to HCO_3^- for each Ca^{2+}-ion released into the solution. Therefore the straight line reaching equilibrium at point CA represents the chemical evolution of the solution flowing along the fracture under closed system conditions. At some position x_{in} in the fracture due to the additional source of CO_2, the concentration of CO_2 increases from point B′ to point B, and the further chemical evolution will proceed along the full line until it meets the equilibrium curve at point CB. c_{eq1} and c_{eq2} can then be obtained from the $[Ca^{2+}]$ coordinates of the points CA and CB. It should be noted that in all the following model runs point B′ is very close to the equilibrium curve, since the aggressive solution quickly approaches equilibrium.

In our simulation of conduit evolution we have changed the program by using c_{eq1} for the rate law if $x<x_{in}$, and replacing it by c_{eq2} for $x>x_{in}$. Figure 4a shows the breakthrough curves of the flow rates for various values of K for the standard fracture with the parameters of Fig. 2. At $x_{in}=KL$, the initial equilibrium concentration $c_{eq1}=2\cdot10^{-6}$ mol/cm^3 increases by 10% to $c_{eq2}=2.2\cdot10^{-6}$ mol/cm^3. This corresponds to an increase of the CO_2 concentration of $\Delta[CO_2]=3.5\cdot10^{-7}$ mol/cm^3, or expressed as Δp_{CO_2} in equilibrium with the solution of $6.5\cdot10^{-3}$ atm. Note that the breakthrough curve with $K=1$ is the curve of our standard shown by Fig. 2a. All curves exhibit the same behavior. Breakthrough times,

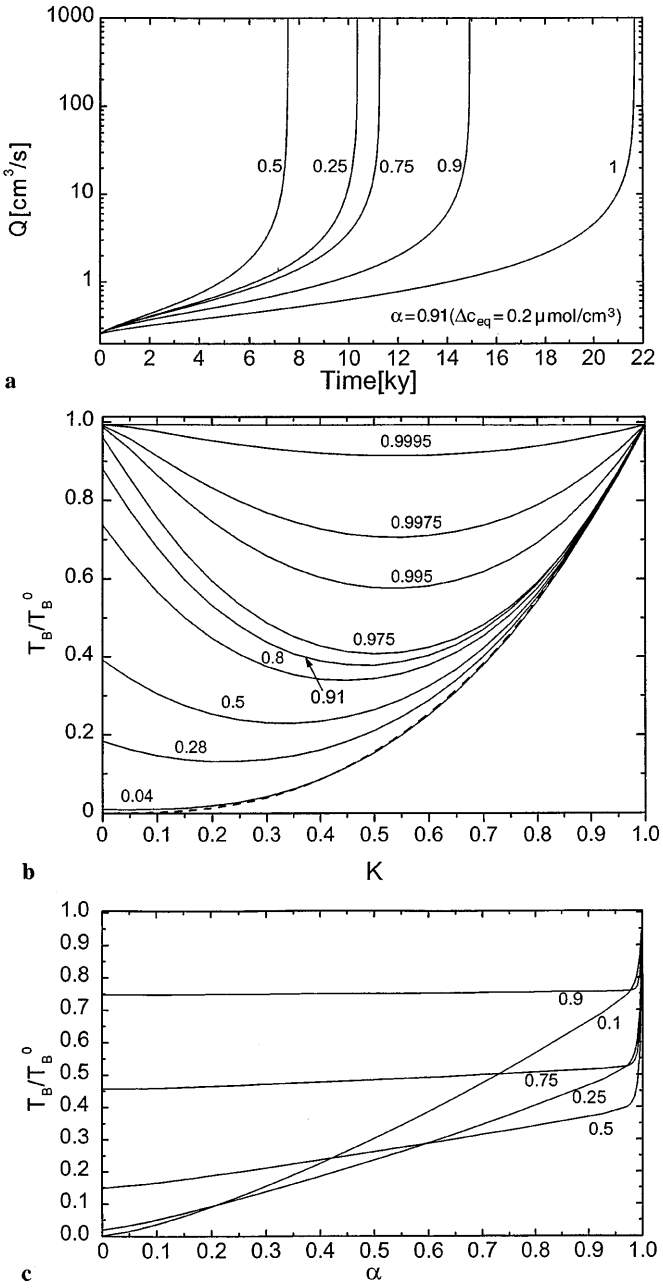

Fig. 4
Breakthrough behavior for point inputs of volcanic CO_2 at $x_{in}=K\cdot L$ for various K. **a** Evolution of flow rates for the standard conduit with a CO_2-input for various values of K (denoted on the curves) $\Delta c_{eq}=0.2\cdot10^{-6}$ mol/cm^3. The curve with $K=1$ corresponds to the standard run of Fig. 2. **b** Breakthrough times as a function of K for various values of $\alpha=c_{eq1}/(c_{eq1}+\Delta c_{eq})=c_{eq1}/c_{eq2}$ (values denoted on the curves). **c** Breakthrough times as a function of α for various values of K (values denoted on the curves). In Fig. 4b and 4c the time scale is in units of the breakthrough time of the fracture without CO_2-supply. In this scale the curve is valid generally. See discussion

however, change from 21700 years ($K=1$) to a minimum value of 7500 at $K=0.5$.

Figure 4b illustrates the breakthrough times for various values of the ratio $c_{eq1}/c_{eq2}=\alpha$ as a function of K. All

curves exhibit a minimum, which depends on α. Note that the breakthrough times at $K=0$ are related to an inflowing solution of c_{eq2}. Therefore these breakthrough times drop with increasing c_{eq2} according to Eq. 3 by $T_B=\alpha^{4/3}\cdot T_B^0$.

Figure 4c represents the breakthrough times for various K as a function of α. In all cases there is a drastic drop in breakthrough times even for relatively small values of Δc_{eq}, i.e. $\alpha\approx 0.91$. Two sets of curves are observed. For $K>0.5$ the breakthrough times drop by up to a factor of two for $\Delta c_{eq}\approx 0.5\cdot 10^{-7}$ mol/cm^3 ($\alpha=0.975$). But then little variation is observed. In contrast the breakthrough times show a significant continuous decrease for $K<0.5$. To elucidate this behavior we have calculated the dissolution rates along the fracture for $K=0.75$ and $K=0.25$ for various times of their evolution ($\Delta c_{eq}=2\cdot 10^{-7}$ mol/cm^3, $\alpha\approx 0.91$). This is shown by Fig. 5. The dashed lines represent the situation for $K=0.25$. At the onset of karstification the dissolution rates exhibit a characteristic drop close to the entrance until they are boosted up at $x_{in}=25\,000$ cm. Then once again the rates drop until they attain their lowest value at the exit. Therefore during the entire time span of their evolution the rates at the exit are significantly lower than those for $x<x_{in}$ and the restriction to the flow rates is caused by the bottleneck due to the narrow exit. This can visualized from Fig. 6, which illustrates the aperture width profiles of the fracture. It is of utmost importance to realize that the positive feedback loop is operative at the most restricted section of the conduit, since Hagen-Poisseuilles law relates the flow rates in laminar flow to $1/a^3$. Therefore the most restricted section determines flow resistance, and breakthrough times decrease if these sections become shorter (cf. Eq. 3). This is the reason, why breakthrough times decrease with increasing values of K. For some value of K, a minimum will occur, when the first section $0<x<x_{in}$ has attained a flow resistance comparable to the section from $x_{in}<x<L$. As long as the last section

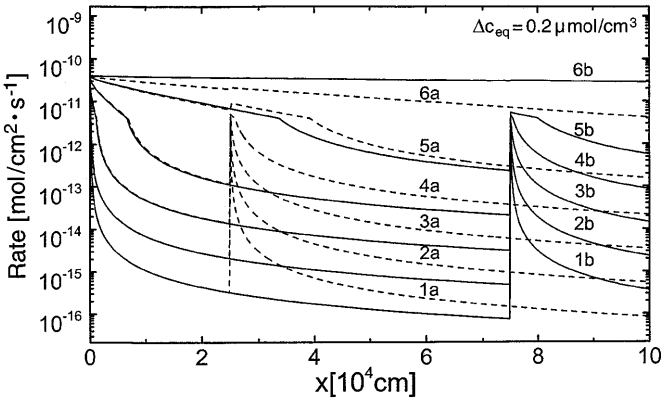

Fig. 5
Dissolution rates for the point CO_2 input at $K=0.25$ (*dashed lines*) recorded at 0.1, 6.5, 9.4, 10.13, 10.35, 10.39 ky (labelled from 1a–6a respectively) and the for the input at $K=0.75$ (*full lines*) recorded at 0.1, 6.93, 10.19, 11.07, 11.27, 11.31 ky (labelled from 1b–6b respectively)

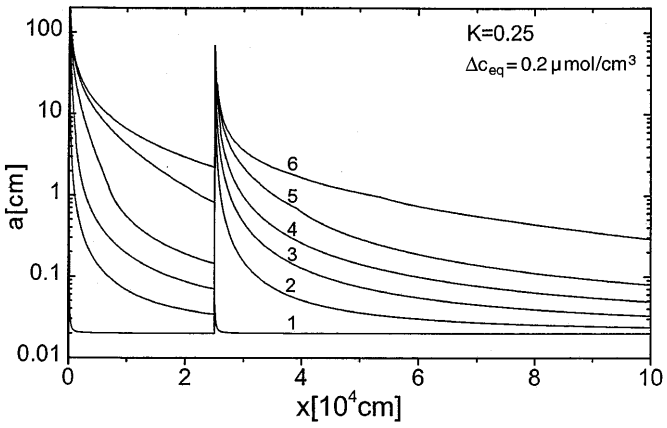

Fig. 6
Profiles of aperture widths for the input of CO_2 at $K=0.25$, recorded at the times given in Fig. 5, labelled from 1–6

controls the flow rates due to a sufficiently large resistance, breakthrough times are sensitive to an increase in c_{eq2}, which causes an increase in the dissolution rates at the exit. Therefore, with increasing c_{eq2}, a continuous drop of breakthrough times occurs as depicted in Fig. 4. The situation becomes different for $K=0.75$. The dissolution rates, as they develop in time along the fracture are also drawn in Fig. 5 (full lines). They first follow the rates as in the case of $K=0.25$, but drop further until they are boosted up at $x_{in}=75\,000$ cm ($K=0.75$). Now the rates at the exit are higher during almost the entire time span until breakthrough is achieved. Consequently the most restricted part of the fracture is in the region from $0<x<x_{in}$. Therefore increasing K leads to an increase in breakthrough times due to the increasing resistance of the restricted part. For further illustration Fig. 7 shows the corresponding aperture width profiles along the fracture. The first part of the fracture now represents the bottleneck. An increase in Δc_{eq} only affects the rates at the exit, but has no influence to the rates in the restricted part for $x<x_{in}$. Therefore an increase of Δc_{eq} by an input of CO_2 is only effective as long as the resulting Δc_{eq} is needed to widen the exit part such that its resistance becomes sufficiently small compared to that of the first part. A significant drop of breakthrough times occurs already for small values of Δc_{eq}. A further increase of Δc_{eq} is then of little influence, since once the exit part has attained a sufficiently small resistance, breakthrough is determined entirely by the first part.

In summary we state: If an extra CO_2-source supplies small amounts of CO_2 , sufficient to an increase of p_{CO_2} by only $2\cdot 10^{-3}$ atm, breakthrough times are already significantly reduced. This is particularly true for the values of $K\leq 0.5$. In this case, as can be visualized by Fig. 3, the total pressure of CO_2 in equilibrium with the solution is about 0.02 atm, which is a surprisingly low value. In other words, very small quantities of volcanic CO_2 are already sufficient to reduce breakthrough times considerably. We have modeled the reduction of breakthrough times

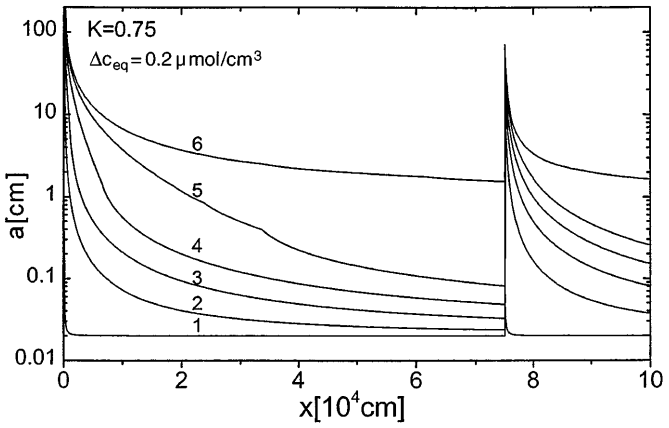

Fig. 7
Profiles of aperture widths for the input of CO_2 at $K=0.75$, recorded at the times given in Fig. 5, labelled from 1–6

for $c_{eq1}=1$ μmole/cm^3. This is the case in poorly vegetated karst surfaces. Since the reduction of breakthrough times depend on $\alpha=c_{eq1}/(c_{eq1}+\Delta c_{eq})$, a reduction of c_{eq1} reduces also the value Δc_{eq} to effect a similar influence on breakthrough.

Extended sources of CO_2

To simulate CO_2-sources by microbiological activity we assume that an evenly distributed population of microorganisms oxidizing organic carbon and O_2 into CO_2 live in the fractures. They deliver a constant rate of CO_2 as long as a sufficient amount of oxygen and organic matter is available. We therefore model this situation by a linear increase of c_{eq} from c_{eq1} to c_{eq2} from the entrance $x=0$ to $x_m=KL$. For $x>x_m$, c_{eq} stays constant. Solubility of oxygen in water at 10 °C is about 11.3 mg/l. The lowest concentration at which aerobic bacteria can still exist is about 0.05 mg/l (Freeze and Cherry 1979). Therefore the maximal increase of concentration in CO_2 by biological activity is about $3.5\cdot10^{-7}$ mol/cm^3. This corresponds to a change of concentration by $\Delta c_{eq}\approx2\cdot10^{-7}$ mol/cm^3, when $c_{eq1}=2\cdot10^{-6}$ mol/cm^3. Extended supply of CO_2 can also result by migration of endogenic CO_2 from the deep underground.

We have modelled the evolution of our standard fracture ($c_{eq1}=2\cdot10^{-6}$ mol/cm^3) for Δc_{eq} between $1\cdot10^{-8}$ mol/cm^3 up to $2\cdot10^{-7}$ mol/cm^3. Figure 8a displays the K-dependence of the breakthrough times for various values of Δc_{eq}. With increasing K a significant reduction is observed, which goes far beyond that when CO_2 is supplied at a point input (cf. Fig. 4a). Figure 8b represents the breakthrough times as a function of Δc_{eq} for various values of K (denoted at the curves). There is a steep decrease at low Δc_{eq}. Most of the reduction occurs for $\Delta c_{eq}\le5\cdot10^{-8}$ mol/cm^3. Thus microbiological activity, where the organism dwell in the first half of the fracture

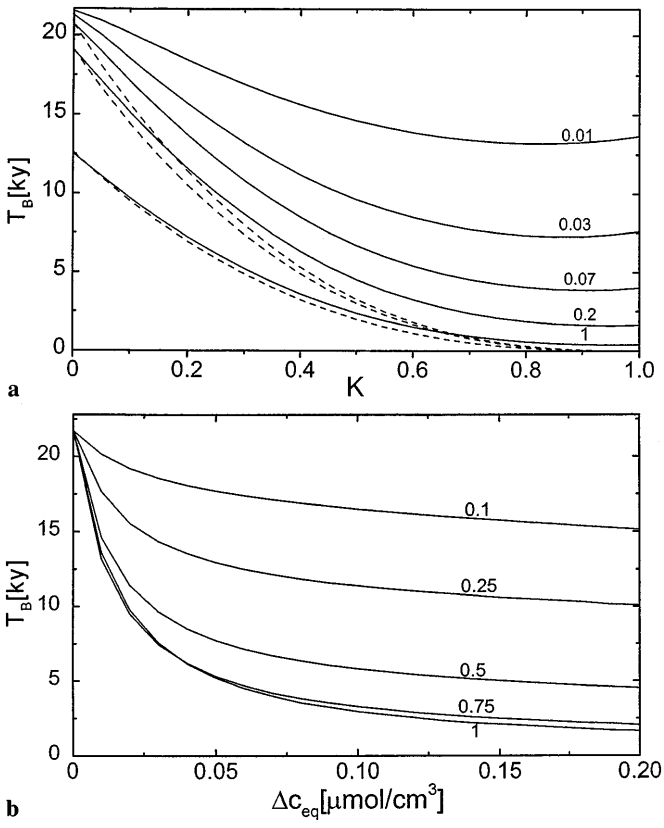

Fig. 8
Breakthrough times for the standard fracture with continuous CO_2-input from $x=0$ to $x=KL$ for various values of K. **a** Breakthrough times as a function of K for various Δc_{eq} denoted in units of 10^{-6} mol/cm^3 at the curves. The *dashed curves* depict theoretical approximations given in the discussion (Eq. 15). For $\Delta c_{eq}\ge1$ μ mol/cm^3 this approximation is quite accurate, but deviations from the numerical calculation are significant for lower values. The *lowest dashed curve* is for $\Delta c_{eq}=1$ μmol/cm^3, the next one for $\Delta c_{eq}=0.2$ μmol/cm^3 and the upper one for $\Delta c_{eq}=0.07$ μmol/cm^3. **b** Breakthrough times as a function of Δc_{eq} for various K, denoted on the curves

($K=0.5$) and only about 25% of the maximal available CO_2 is consumed, reduces breakthrough time from 21700 years to 7500 years. If only 10% of O_2 has been used ($\Delta c_{eq}=2.5\cdot10^{-8}$ mol/cm^3) the reduction is still to 10000 years.

To envisage the evolution of the conduit, Fig. 9 shows the dissolution rates along the fracture for various times. There is a steep decrease in rates at the entrance. But then the rates become constant due to the linear increase in c_{eq}, which compensates their decrease due to the increasing concentration c. At $x_m\ge0.5\,L$, c_{eq2} remains constant and the rates drop continuously when the solution moves towards the exit. Figure 10 shows the corresponding aperture width profiles. The bottleneck to flow is located at the exit. Therefore the widening there, determines the breakthrough time.

In this scenario we have assumed that microbiological oxidation of organic carbon increases with increasing

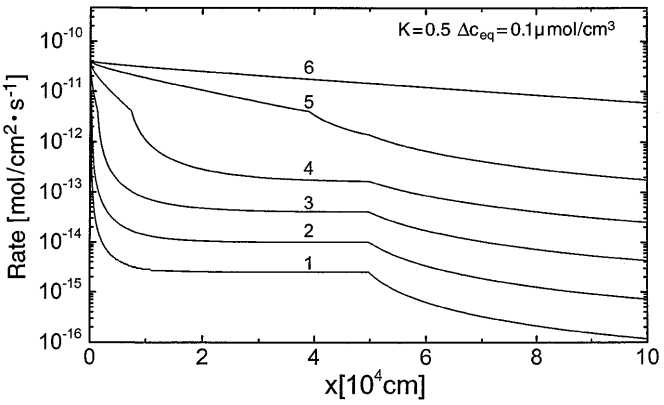

Fig. 9
Dissolution rates for extended CO_2 input in the standard fracture; $K=0.5$, $\Delta c_{eq}=0.1\cdot 10^{-6}$ mol/cm^3. Profiles are recorded at 0.1, 3, 5, 5.7, 5.82, 5.83 ky, labelled from 1–6 respectively

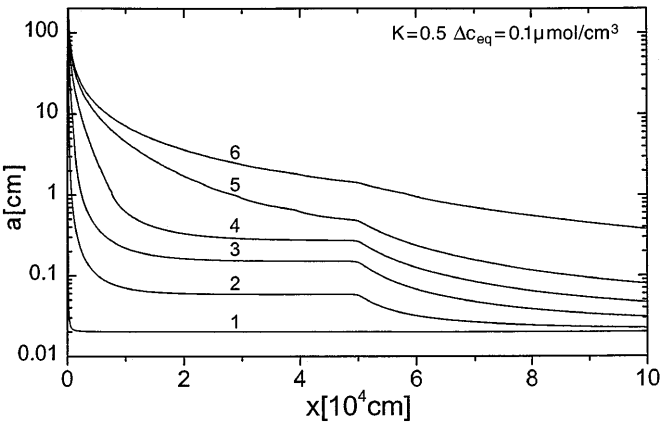

Fig. 10
Aperture widths for the example from Fig. 9, recorded at the same time as in Fig. 9

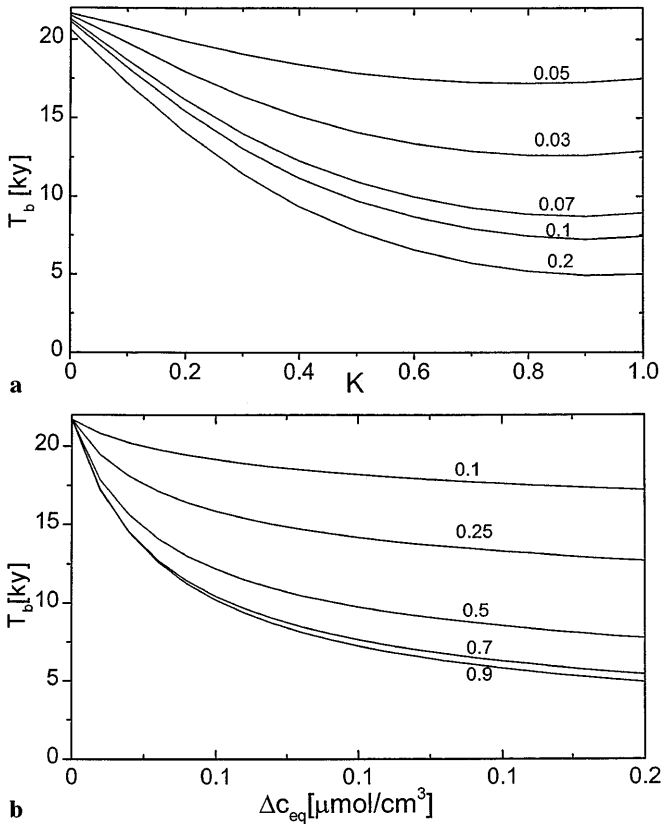

Fig. 11
Breakthrough times for the standard fracture with continuous CO_2-input from $x=0$ to $x=KL$ for various values of K. CO_2-input decreases with time, so that $\Delta c_{eq}(t)=\Delta c_{eq}(0)\,Q(0)/Q(t)$. **a** Breakthrough times as a function of K for various Δc_{eq}, denoted on the curves in units of 10^{-6} mol/cm^3. **b** Breakthrough times as a function of Δc_{eq} for various K, denoted on the curves

flow through the fracture, such that the increase in Δc_{eq} is independent on the flow rate. This implies that the overwhelming part of bacteria is floating in the solution and their concentration is independent of flow rate. If, however, the bacteria are located at the fissure surfaces forming a biofilm and their rate of CO_2-production is assumed to be constant, then the concentration of CO_2 decreases when the flow rate increases. If at time $t=0$, $\Delta c_{eq}(0)$ is the increase in equilibrium concentration with respect to calcite at flow rate $Q(0)$, at later times t, $\Delta c_{eq}(t)=\Delta c_{eq}(0)\cdot Q(0)/Q(t)$, where $Q(t)$ is the flow rate at time t. This can be incorporated into the numerical model by employing $\Delta c_{eq_2}(t)$ in each time step. The results are shown by Fig. 11a and b. Qualitatively they resemble those of Fig. 8, although the variations are less pronounced.

Many different scenarios can be envisaged and easily be incorporated into the numerical model. A scenario, which could apply to extended release of volcanic CO_2 or also to microbial production, is the following. From $x_1=K_1L$ to $x_2=K_2L$, a constant rate of CO_2 is supplied, until $c_{eq2}=c_{eq1}+\Delta c_{eq}$. Thus at a constant rate of CO_2-supply, there is a linear increase in c_{eq} in this region between x_1 and x_2. For $x>x_2$, c_{eq_2} remains constant. Figure 12a and b show the results for the standard conduit ($K_1=0.3$, $K_2=0.8$, $\Delta c_{eq}=1\cdot 10^{-7}$ mole/cm^3). Breakthrough is achieved at 3300 years, a reduction by almost a factor of 7. Figure 12a illustrates the dissolution rates at various times. After an abrupt drop close to the entrance the rates increase in the region, where CO_2 is released, and then drop when approaching the exit. The resulting aperture width profiles are depicted in Fig. 12b.

Discussion

So far we have given only a few idealized examples related to the standard fracture, which demonstrate the underlying processes. It would be useful, however, to obtain information about their general validity with respect to variation of the parameters determining the geological situation (cf. Eq. 3). These are the fracture aperture width

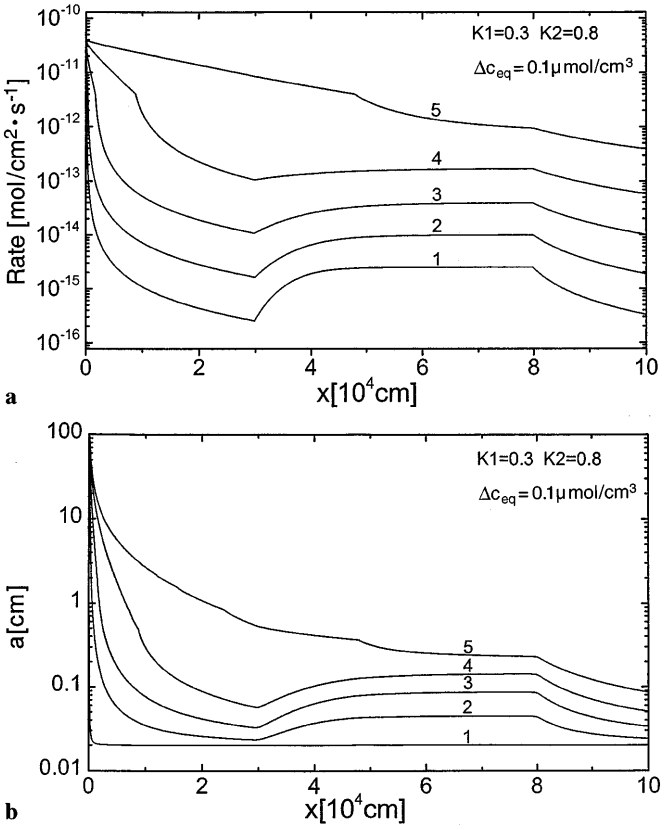

Fig. 12
Standard fracture with continuous CO_2-input between $x_1 = 0.3L$ and $x_2 = 0.8L$, $\Delta c_{eq} = 0.1 \cdot 10^{-6}$ mol/cm^3. The profiles are recorded at 0.1, 2, 2.93, 3.21, 3.29 ky, labelled from 1–5 respectively. **a** Dissolution rates along the fracture. Note the changes at x_1 and x_2. **b** Aperture widths along the fracture

a_0, the length L, the hydraulic gradient i, and furthermore the chemical parameters in Eq. 3.
In order to give at least an estimation of breakthrough times one has to know the dissolution rates at $x = KL$, where the equilibrium concentration is still c_{eq1}, and also at the exit of the fracture, where $c_{eq} = c_{eq2}$. These rates can be obtained from a differential equation for the concentration $c(x)$, which can be derived from mass conservation (Dreybrodt 1990, 1996). It reads

$$\frac{dc(x)}{dx} = F(c(x)) \cdot P(x)/Q, \tag{5}$$

where $F(c(x))$ is the dissolution rate (cf. Eq. 1) by concentration $c(x)$ at location x. Q is the flow rate through the fracture and $P(x)$ its perimeter at the position x. Solving this equation for the initial plane parallel fracture enables one to obtain the required initial dissolution rates. For the initial plane parallel fracture, with $b_0 \gg a_0$ (b_0 is the width of the fracture) these are given by

$$F(x) = k_n \left(1 - \frac{c(x_1)}{c_{eq}}\right)^n \left(1 + \frac{x - x_1}{\lambda}\left(1 - \frac{c(x_1)}{c_{eq}}\right)^{n-1}\right)^{\frac{n}{1-n}}, \tag{6}$$

Dreybrodt (1996). Where x is the distance from the input and $x_1 < x$ is some location where the concentration $c(x_1)$ is known. No CO_2-supply is located between x and x_1. The penetration length λ is given by

$$\lambda = \frac{a_0^3 c_{eq} i \rho g}{24 \eta (n-1) k_n}. \tag{7}$$

Let us first discuss the case of a CO_2 point input at $x = KL$. By use of Eqs. 6 and 7 and considering that $c_{eq} = c_{eq1}$ for $x \le KL$ and c_{eq2} for $x > KL$ one gets

$$F(KL) = k_n \left(1 - \frac{c_s}{c_{eq}}\right)^n \left(1 + \frac{KL}{\lambda}\left(1 - \frac{c_s}{c_{eq}}\right)^{n-1}\right)^{\frac{n}{1-n}}$$

for $x \le KL$ (8a)

Assuming that at $x = KL$ the solution is very close to equilibrium, such that $c_{eq1} - c(KL) \ll c_{eq2} - c_{eq1}$, one gets

$$F(L) = k_n (1-\alpha)^n \left(1 + \frac{(1-K)L}{\lambda}\, \alpha (1-\alpha)^{n-1}\right)^{\frac{n}{1-n}},$$

$$\alpha = \frac{c_{eq1}}{c_{eq2}}. \tag{8b}$$

This assumption holds when the condition $(\lambda / KL) \cdot ((1-\alpha)/\alpha)^{1-n} \ll 1$ is valid, which is true in all cases of interest. The breakthrough times can now be easily calculated, when the rates $F(KL) = F(L)$. In this case the widening of both bottlenecks is equal, and therefore the breakthrough time is minimal. For a given value of α, there exists a value of K_{min}, for which this minimum breakthrough time occurs. From the condition $F(K_{min} L) = F(L)$, and neglecting the summand "1" in the second bracket of Eq. 8a, one obtains

$$K_{min} = ((\lambda/L)(1-\alpha)^{-(n-1)} + \alpha)/(1+\alpha), \tag{9a}$$

which can be approximated by

$$K_{min} = \alpha/(1+\alpha), \text{ if} \tag{9b}$$

$$(\lambda/L)(1-\alpha)^{-(n-1)} \ll \alpha. \tag{9c}$$

Under this condition, $K_{\min}$ becomes independent of the parameter λ/L. The breakthrough time can now be calculated from Eqs. 2 and 8a

$$T_B^{min} = T_B^0 \cdot K_{min}^{n/n-1} = T_B^0 \cdot \left(\frac{\alpha}{1+\alpha}\right)^{n/n-1} \tag{10}$$

Therefore $T_B^{\min}$ has the same dependence on the various parameters as T_B^0.
Another limiting case can also be given: if c_{eq2} becomes so large, that the dissolution rates at the exit are sufficiently high, the last part of the fracture widens quickly in comparison to the first part. Therefore after a short time the hydraulic head acts only along the first part KL of the fracture. The breakthrough time can then be calculated by replacing L by KL, and i by i/K in Eq. 3. One thus obtains

$$T_B^{Lim} = K^{\frac{2n}{n-1}} \cdot T_B^0. \tag{11a}$$

This equation describes exactly the lower dashed curve in Fig. 4b. Finally for $K=0$ we find

$$T_B^{K=0} = \alpha^{\frac{n}{n-1}} \cdot T_B^0, \tag{11b}$$

since in this case c_{eq} equals c_{eq2} along the entire fracture. In all three limiting cases the dependence of T_B on the parameters is given by that of T_B^0. Therefore one can conclude, since all the equations solely contain the algebraic group λ/L, that this is true also generally and one can read T_B, for all intermediate cases from Fig. 4a if T_B^0 is known, provided $n=4$. For other values of n similar graphs can be constructed. In the region between $n=3$ and $n=10$ which is characteristic for natural limestones (Eisenlohr and others 1999) the deviations are not dramatic. We have therefore plotted the breakthrough times as T_B/T_B^0 in Fig. 4.

Now we focus on the case of a continuous CO_2 input, where $c_{eq}(x) = c_{eq1} + \frac{x}{KL}\Delta c_{eq}$ for $x \le KL$ and $c_{eq}(x) = c_{eq1} + \Delta c_{eq}$ for $x > KL$. In this case a special solution of the differential Eq. 5 can be given for $x \le KL$, which is valid for the initial plane parallel fracture. It reads

$$c(x) = c_{eq1} + \frac{x}{KL}\Delta c_{eq} - \beta\left(c_{eq1} + \frac{x}{KL}\Delta c_{eq}\right),\ \beta < 1 \tag{12}$$

In this case the dissolution rates become constant along the fracture as long as $x \le KL$.

$$F(c(x)) = k_n \beta^n \tag{13}$$

This is nicely demonstrated by the profile of the dissolution rates in Fig. 9, which also shows that this special solution becomes valid for solutions entering with a concentration $c(0) < c_{eq1}$ after a short distance. In all cases of interest this distance is small compared to KL.

The value of β is related to Δc_{eq} by

$$\frac{\Delta c_{eq}}{c_{eq1}} = \frac{KL}{\lambda}(n-1)\beta^n/(1-\beta) \tag{14}$$

By use of Eq. 5 it is now possible to calculate the rate at the exit of the initial fracture, and one can compare this initial dissolution rate to that, when no additional CO_2 is supplied. From this we can give an answer to the following important question. Which amount of Δc_{eq} is necessary to lower the breakthrough time significantly? Figure 8b suggests that this value can be quite low ($\Delta c_{eq}/c_{eq1} \approx 0.025$). Since the breakthrough times are related to the initial dissolution rates at the evolving bottleneck of the conduit (in this case the exit), one can compare these initial rates for the case with CO_2-supply to those without. From Eq. 2 one concludes that if the rates with CO_2 supply exceed those without by a factor of two, then the breakthrough times are reduced accordingly. This leads to an analytical equation (not given here) which can be solved numerically. It must be noted, that this equation contains only the parameter groups L/λ, $\Delta c_{eq}/c_{eq1}$, and K. By solving this equation one therefore obtains, as a function of K and L/λ, the value of $\Delta c_{eq}/c_{eq1} = \varepsilon_{crit}$, which is necessary to reduce breakthrough times to about one half of those without CO_2-supply. The results are shown in Fig. 13 for various values of L/λ denoted at the corresponding curves. The lowest value of L/λ corresponds to a fracture with $a_0 = 0.04$ cm, $L = 10^4$ cm, $i = 0.05$, whereas the highest value represents a fracture with $L = 10^6$ cm, $a_0 = 0.01$ cm and $i = 0.01$. Thus the region of L/λ given in Fig. 13 covers the entire region of natural karstification. The middle curve represents the standard fracture of Fig. 2.

The four dashed lines parallel to the K-axes represent the maximal possible values of $\varepsilon_{max} = \Delta c_{eq}^{max}/c_{eq1}$, which can result by microorganisms, when using up all available O_2, thus creating an increase of CO_2 concentration by 0.35 μmol/cm^3. This corresponds to Δc_{eq} of 0.32 μmol/cm^3 at $c_{eq1} = 0.5$ μmol/cm^3, 0.3 μmol/cm^3 at $c_{eq1} = 1$ μmol/cm^3, 0.2 μmol/cm^3 at $c_{eq1} = 2$ μmol/cm^3, and 0.1 μmol/cm^3 at $c_{eq1} = 4$ μmol/cm^3 correspondingly (cf. Fig. 3).

If the curves representing ε_{crit} lie above the corresponding lines for ε_{max}, karstification is not significantly enhanced by organic CO_2 supply. If, however, the curves are below, a drastic enhancement is to be expected. Furthermore from Fig. 13 one deduces that a deep invasion of microorganisms into the fracture is necessary. In view of the initial flow velocities of the water ($v \approx 10^4 \cdot a_0^2 i$ [cm/s]) in the order of several meters/day such deep invasion seems likely. For the standard case, $c_{eq1} = 2$ μmole/cm^3, $K > 0.4$ is required. If little external CO_2 is supplied from the surface, i.e. $c_{eq1} = 0.5 - 1$ μmole/cm^3, this value of K is reduced and significant enhancement of karstification can arise by solely the activity of microorganisms.

It is also possible to give the extreme limit of enhancement for each value of K. If Δc_{eq} becomes so large that the constant initial dissolution rate becomes very large compared to that of the same fracture with no CO_2-supply, karstification is entirely governed by evolution of the

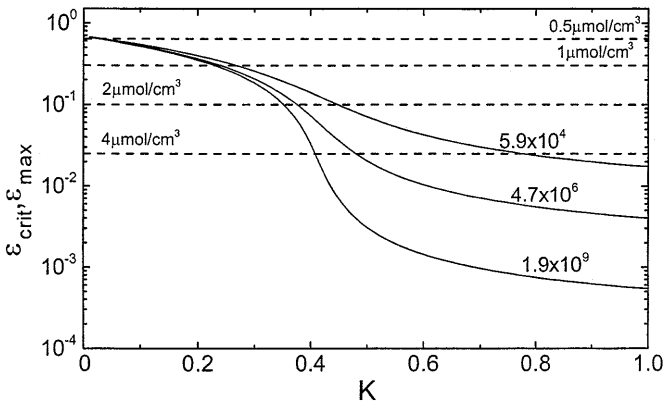

Fig. 13
Limiting curves of ε_{crit} for various values of L/λ denoted at the curves. The dashed lines give the value of ε_{max} originating from microbial activity in a solution of equilibrium concentration c_{eq} denoted on these lines. Whenever the curves for ε_{crit} are below the corresponding line for ε_{max} karstification is significantly enhanced

last part of the fracture which represents the bottleneck for the flow ($x>KL$). Then the hydraulic head acts entirely along that part and by use of Eq. 3 one finds

$$T_B(K) = T_0(c_{eq2}) \cdot (1-K)^{\frac{2n}{n-1}} \quad (15)$$

$T_0(c_{eq2})$ is the breakthrough time of the corresponding fracture with constant $c_{eq} = c_{eq2}$ and can be obtained from Eq. 3.

The lowest dashed curve in Fig. 8a represents this limit, for the standard fracture. It shows that bacterial activity can be sufficient to approach this limit closely. It should be noted that the approximation breaks down for values of K close to 1. For $K=1$ the breakthrough time is given by the dissolution rates at the exit and can be obtained by use of Eqs. 2, 13 and 14. The two higher dashed curves show that for smaller values of Δc_{eq} significant deviations occur.

To summarize the effect of CO_2-supply, Fig. 14 represents its effect for various values of L and K, for the standard fracture otherwise. It demonstrates clearly that for large $L>1$ km and $K>0.5$ an increase of Δc_{eq} by 1 μmol/cm^3 is sufficient to reach the maximum of enhancement. For karstification along short fractures of about 100 m, however, biogenic CO_2 reduces the breakthrough time only to about one half. For low values of $K \approx 0.1$ no significant enhancement arises at all. This again shows that deep invasion of microorganisms into the initial karst system is necessary.

All considerations so far base on the well founded assumption that breakthrough times are governed by widening of that part of the fracture, which exhibits the lowest dissolution rates, such that it evolves into the bottleneck for flow.

This can be nicely demonstrated by Fig. 15. Here we have plotted the results of our standard case from Fig. 8a (full lines). The dotted lines represent correspondingly breakthrough times for the case where the CO_2-supply starts at $x=KL$, i.e. $c_{eq}=c_{eq1}$ for $x \le KL$, and a continuous supply of CO_2 exists for $x>KL$. The numbers on the curves denote $\Delta c_{eq}/c_{eq1}$. For the first case the bottleneck is the back part with the fracture of the length $(1-K)L$. The breakthrough times therefore are some function $f(1-K)$. If, however, CO_2-supply is delivered for $x>KL$, than the front part of the fracture represents the bottleneck and the breakthrough time is a similar function, but now of K, i.e. $f(K)$. At $K \approx 0.5$ breakthrough times should not differ much. Moreover the corresponding curves should be mirror-like, because breakthrough times should be close to each other if the lengths of the bottlenecks are equal for the two cases. As an example, breakthrough time for CO_2-supply at the front part up to $x=KL$, should be equal to the breakthrough time if CO_2 is delivered in the backpart ($x>(1-K)1\ L$), because the lengths of the both bottlenecks are then equal. This behavior is nicely demonstrated by Fig. 15 and gives further support to our crucial assumption.

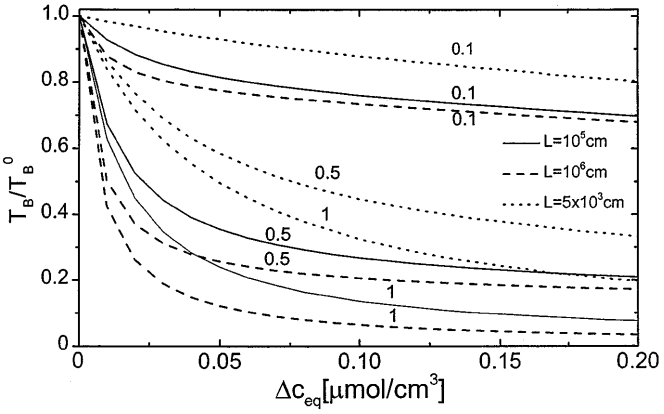

Fig. 14
Breakthrough times for the standard fracture (*full line*) and two fractures with $L=10^6$ cm (*dashed*) and $L=5\cdot10^3$ cm (*dotted*; all other parameters are the same) as function of Δc_{eq}. The numbers on the curves denote K. The time scale is in units of the breakthrough times of the respective fractures without CO_2-supply. These are T = 0.32ky, T = 21.7ky and T = 467ky, for $L=5\cdot10^3$ cm, $L=10^5$ cm and $L=10^6$ cm correspondingly

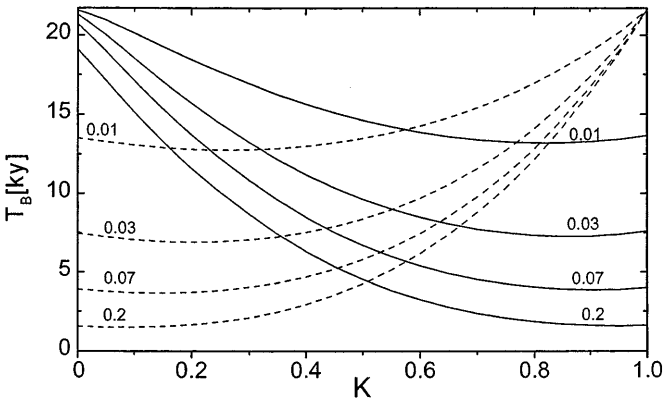

Fig. 15
Breakthrough times of the standard fracture with continuous CO_2-supply in Fig. 8a (*full lines*) compared to those, where a corresponding continuous CO_2 input starts at $x=KL$ (see text)

Conclusion

Subterranean sources of CO_2, either supplied at punctual inputs or continuously along parts of a karstifying fracture, do exert significant influence on the breakthrough times of karstification. In the case of point inputs, a significant reduction of breakthrough times is effected for inputs located near to the center of the fracture. In this case a small increase in the p_{CO_2} of the solution by about $2\cdot10^{-3}$ atm is sufficient to reduce breakthrough times to about a half. A further increase to p_{CO_2} values of 0.06 atm reduces the breakthrough times to about one third compared to those without CO_2-supply. If the location of the CO_2 input is close to the entrance, a large increase of p_{CO_2} to about 0.1 atm is needed for a significant reduction of breakthrough times. For inputs close to the exit

of the fracture even a large increase of p_{CO_2} effects breakthrough times only moderately. The examples above hold for situations of vegetated karst areas, where saturation of emerging karst waters is about 2 μmol/cm^3. For bare karst areas, with saturation of about 0.5–1 μmol/cm^3, the influence of subterranean CO_2 is increased and accordingly less elevation in CO_2-concentration is needed. Continuous CO_2-input may arise from extended diffuse gas migration from deep volcanic sources or by aerobic microorganisms dwelling at the walls of the initial fractures. In the latter case if all oxygen, available in the inflowing water is employed by these organisms, an increase in p_{CO_2} of about $6 \cdot 10^{-3}$ atm results. In all cases of natural karstification this is sufficient to reduce breakthrough times substantially, provided the microorganisms have invaded deep into the fracture, populating at least the first third of its length. If microorganic activity is restricted close to the entrance, only moderate reductions of breakthrough time occur. The influence of microorganic CO_2-supply increases for bare karst areas with little external supply of CO_2, such that karstification can arise if only atmospheric CO_2 ($p_{CO_2} = 3.5 \cdot 10^{-4}$ atm) is contained in the inflowing water. Therefore the consideration of microbiological processes becomes an important new parameter, when discussing karstification. Although little is known about population by microorganisms in initial primary fractures, our model forecasts their influence on karst systems if only a few parameters are known. These are the depth of the invasion into the fracture and the amount of CO_2 released. Furthermore any scenario on subterranean CO_2-inputs can be modeled by our method, such as any combination of point and continuous inputs, and also any local variation of CO_2-supply in different parts of the fracture. This covers most scenarios which can be envisaged from volcanic CO_2-sources, as well as those from microbial activity and any combination of both.

Acknowledgement F.G. thanks the University of Bremen for financial support.

References

Dreybrodt W (1998) Principles of karst evolution from initiation to maturity and their relation to physics and chemistry. In: Yuan Daoxian, Liu Zaihua (eds). Global Karst Correlation. Science Press, Beijing, New York: VSP Utrecht, Tokyo

Dreybrodt W (1996) Principles of early development of karst conduits under natural and man-made conditions revealed by mathematical analysis of numerical models. Water Resour Res 32:2923–2935

Dreybrodt W (1988) Processes in karst systems – physics, chemistry and geology. (Springer Series in Physical Environments 4) Springer, Berlin Heidelberg New York

Dreybrodt W (1990) The role of dissolution kinetics in the development of karstification in limestone. A model simulation of karst evolution. J Geol 98:639–655

Dreybrodt W, Eisenlohr L (1999) Limestone dissolution rates in karst environments. In: Klimchouk A, Ford DC, Palmer AN, Dreybrodt W (eds) Speleogenesis: evolution of karst aquifers. Nat Speleol Soc USA

Dreybrodt W, Gabrovsek F (1999a) Dynamics of the evolution of a single karst conduit. In: Klimchouk A, Ford DC, Palmer AN, Dreybrodt W (eds) Speleogenesis: evolution of karst aquifers. Nat Speleol Soc USA

Dreybrodt W, Gabrovsek F (1999b) Influence of fracture roughness on karstification times. In: Klimchouk A, Ford DC, Palmer AN, Dreybrodt W (eds) Speleogenesis: evolution of karst aquifers. Nat Speleol Soc, USA

Dreybrodt W, Siemers J (1999) Cave evolution on two-dimensional networks of primary fractures in limestone. In: Klimchouk A, Ford DC, Palmer AN, Dreybrodt W (eds) Speleogenesis: evolution of karst aquifers. Nat Speleol Soc, USA

Eisenlohr L, Madry B, Dreybrodt W (1997) Changes in the dissolution kinetics of limestone by intrinsic inhibitors adsorbing to the surface. In: Proceedings of the 12th Int. Cong. of Speleology, La Chaux de Fonds, Switzerland. La Chaux de Fonds, Switzerland, vol II, pp 81–84

Eisenlohr L, Meteva K, Gabrovsek F, Dreybrodt W (1999) The inhibiting action of intrinsic impurities in natural calcium carbonate minerals to their dissolution kinetics in aqueous H_2O-CO_2 solutions. Geochim Cosmochim Acta 63:989–1001

Felip M, Pace ML, Cole JJ (1996) Regulation of planktonic bacterial growth rates: The effects of temperature and resources. Microb Ecol 31:15–28

Ford DC, Williams PW (1989) Karst Geomorphology and Hydrology. Unwin Hyman, Boston

Freeze RA, Cherry HA (1979) Groundwater. Prentice-Hall, Englewood Cliffs

Groves CG, Howard AD (1994a) Minimum hydrochemical conditions allowing limestone cave development. Water Resour Res 30:607–615

Groves CG, Howard AD (1994b) Early development of karst systems. 1 Preferential flow path enlargement under laminar flow. Water Resour Res 30:2837–2846

Howard AD, Groves CG (1995) Early development of karst systems. 2 Turbulent flow. Water Resour Res 31:19–26

Kazumi J, Capone DG (1994) Heterotrophic microbial activity in shallow aquifer sediments of Long Island. Microb Ecol 28:19–37

Leichtfried M (1995) Organic matter in bedsediments – an energy source for lotic ecosystems (a compilation of a long-term study). Folia Fac Nat Univ Masarykianae, Biologia 91, 1995:77–93

Menne B (1997a) Sessile Mikrobiologie (Myxobakterien) im hochphreatisch-hydroklasalen Raum der Rettenbachhöhle, Stichprobenerhebungen im Einzugsgebiet. Projekt Karstdynamik des Nationalparks Kalkalpen GmbH, Oberösterreich, Teilprojekt 7.5.3 Mikrobielle Analytik III. Mühlacker/Molln

Menne B (1997b) Mikrobiologische Aktivität auf Karstgestein. Erdwissenschaftliche Aspekte des Umweltschutzes. 4. Arbeitstagung des Bereiches Umwelt, Tagungsband, Wien, pp 121–126

Menne B (1998) Carbonatolyse und Biokonservierung als Mechanismen der Verkarstung und Speleogenese. Beitr Hydrogeol (in press)

Menne B, Rückert G (1988) Myxobakterien (Myxobacterales) in Höhlensedimenten des Hagengebirges (Nördliche Kalkalpen). Die Höhle 39:120–31

Morita RY (1985) Starvation and miniaturization of heterotrophs with special emphasis on maintenance in the starved viable state. In: Fletcher M, Floodgate G (eds) Bacteria in their natural environments: the effect of nutrient conditions. Soc Gen Miocrobiol, UK, pp 111–130

Palmer AN (1984) Recent trends in karst geomorphology. J Geol Educ 32:246–253

Palmer AN (1991) The origin and morphology of limestone caves. Geol Soc Am Bull 103:1–21
Palmer AN (1999) Digital modelling of individual solution conduits. In: Klimchouk A, Ford DC, Palmer AN, Dreybrodt W (eds) Speleogenesis: evolution of karst aquifers. Nat Speleol Soc, USA
Shang C, Caldwell DE, Stewart JWB, Tiessen H, Huang PM (1996) Bioavailability of organic and inorganic phosphates adsorbed on short-range ordered aluminium precipitate. Microb Ecol 31:29–39
Siemers J, Dreybrodt W (1998) Early development of karst aquifers on percolation networks of fractures in limestone. Water Resour Res 34:409–419
White WB (1988) Geomorphology and hydrology of karst terrains. Oxford Univ Press, New York